

# Cohesive energies in the Al-Co binary alloy system

M. Mihalkovič\* and M. Widom  
*Department of Physics, Carnegie Mellon University*  
*Pittsburgh, PA 15213*  
 (Dated: August 22, 2005)

The phase diagram of the Al-Co binary alloy system is intensively studied because of its importance for understanding decagonal quasicrystals, but remains imprecisely known due to the occurrence of many competing complex structures with composition close to  $\text{Al}_{13}\text{Co}_4$ . We apply first-principles total energy calculations to compare the cohesive energies of known and hypothetical structures. Our results confirm the experimentally established phase diagram in every detail except near  $\text{Al}_{13}\text{Co}_4$ , where the reported phases (Pearson symbols mC102 and oP102, both well known decagonal quasicrystal approximants) turn out to be unstable at low temperatures. They may be stabilized at high temperatures by the entropy of Aluminum vacancy hopping and low frequency vibrational modes. A subset of Al atoms displays nearly liquid diffusive motion.

PACS numbers:

## I. INTRODUCTION

Decagonal quasicrystals occur as metastable phases in the binary alloy Al-Co [1] and as stable phases in the Al-Co-Ni ternary[2]. Knowledge of the complete phase diagrams of these alloy systems can aid understanding of the structures and stability of the quasicrystals. Unfortunately, but not surprisingly, these phase diagrams remain poorly understood precisely at the compositions of greatest importance, with a proliferation of competing and imperfectly characterized crystal structures. Some of these structures are quasicrystal approximants, which means that they are crystals containing local structures that can be extended quasiperiodically to match the global quasicrystal structure.

The regime  $0.23 < x_{\text{Co}} < 0.26$  is the most controversial with the various experimentally observed phase diagrams differing in the total number of phases and the composition sequence in which they occur [3–9]. Even the most recent of these are of questionable validity because they violate the “rule of thumb” that phases close in composition should not coexist over an extended temperature range [10]. Our calculations suggest revisions in the assessment of low temperature stability, where experiments are unreliable due to diverging equilibration times.

The most recent experimental determinations agree on the identities and approximate structures of the phases, but not their sequence. According to Grushko [9], starting from pure Al.cF4 (LT), they are: Al9Co2.mP22 (LT); O- $\text{Al}_{13}\text{Co}_4$ .oP102 (LT); M- $\text{Al}_{13}\text{Co}_4$ .mC102 (LT); Y- $\text{Al}_{13}\text{Co}_4$ .mC34-1.8 (HT); Z- $\text{Al}_3\text{Co}$  (LT); Al5Co2.hP28 (LT); AlCo.cP2 (LT); Co.hP2 (LT). Goedecke and Ellner [5] interchange the relative composition of the M- and Y- $\text{Al}_{13}\text{Co}_4$  phases, suggesting that M- $\text{Al}_{13}\text{Co}_4$  is Co-richer than Y- $\text{Al}_{13}\text{Co}_4$ . Neither Y- nor Z- have rigor-

ous structure determinations. However, the structure types are agreed on, with Y- of structure similar to Al13Os4.mC34, though probably with about 1.8 Al vacancies per cell, similar to Al75Co22Ni3. The structure of the Z-phase is known to be a quasicrystal approximant and is sometimes called  $\tau^2$ - $\text{Al}_{13}\text{Co}_4$ .

We apply first-principles total energy calculations to compare cohesive energies of known and hypothetical structures (Fig. 1). Our calculational methods are discussed in section II. The alloy phase diagram at low temperature consists of structures whose energies form the convex hull of cohesive energy as a function of composition. Although our focus is on the Al-Co binary system, we exploit knowledge of the Al-Co-Ni ternary in this study. The known complex quasicrystal approximant phases with composition close to  $\text{Al}_{13}\text{Co}_4$  (Pearson symbols oP102 [11] and mC102 [12, 13]), previously believed stable down to low temperatures, are actually either metastable or stable only at high temperature.

Our main goal is to explain the stability of  $\text{Al}_{13}\text{Co}_4$ , which must be due to some entropic effect. We examine possible sources of entropy including, disorder in “puckering” pattern (section III B), vacancy disorder (section III A), and vibrational entropy (section IV). Our results show that a combination of vacancy and vibrational entropy may be sufficient to stabilize  $\text{Al}_{13}\text{Co}_4$  at high temperatures. We then perform a high temperature molecular dynamics simulation (section V) that suggests the vacancies and vibrations combine to create a nearly liquid diffusive behavior among a subset of Al atoms.

Another reported structure,  $\text{Al}_3\text{Co}$ .oI96, which had previously been presumed metastable??, turns out to be preferred and may be the true low temperature state. Although structurally related to the mC102/oP102 phases, oI96 is not itself a “good approximant”. While oP102 and mC102 alternate flat and puckered atomic layers to achieve a periodicity of 8 Å along the pseudo five-fold axes, oI96 alternates flat layers with pairs of puckered layers for a net 12 Å periodicity. It is closely related to a known high temperature phase,  $\text{Al}_{13}\text{Co}_4$ .mC32, which

---

\*Also at Institute of Physics, Slovak Academy of Sciences, 84228 Bratislava, Slovakia

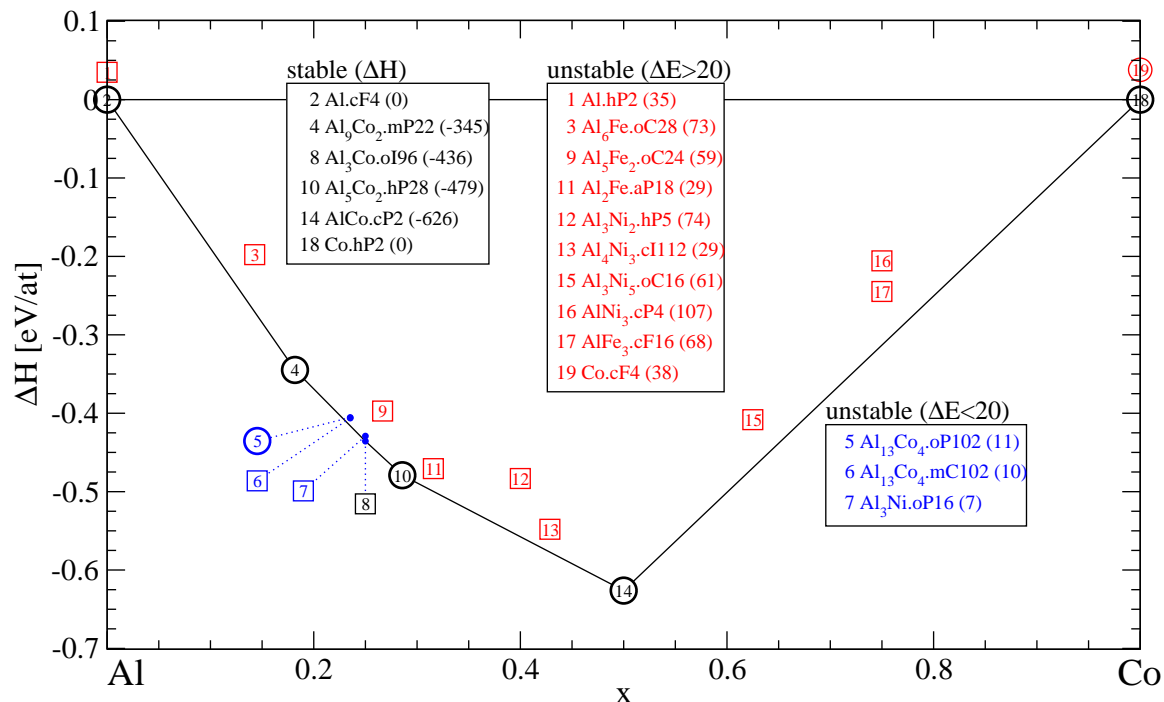


FIG. 1: Enthalpies of formation in the Al-Co binary alloy system over its full composition range. Notation: heavy circles = known (or claimed) low temperature phases, light circles = known high temperature phases, diamonds = known metastable phases, squares = unreported (hypothetical) structures. Structures are labeled by their compound names followed by their Pearson symbols.

has only a 4 Å periodicity, consisting only of flat layers.

## II. METHODS

We calculate total energies within electronic density functional theory using the plane-wave program VASP [14, 15]. Our calculations, which employ PAW potentials [16] in the PW91 generalized gradient approximation [17], are carried out at a fixed cutoff energy of 268 eV. We relax atomic positions and lattice parameters, and select k-point meshes to achieve a target precision of 0.001 eV/atom on all relative energies. More details of similar calculations can be found in Ref. [18].

Structures for study are selected from established experimental phase diagrams [3], collections of intermetallic structures [19] and recent original literature [20]. We name our structures according to the Pearson convention which lists point symmetry, translational symmetry and the number of atomic positions per cell. For example, mC102 is monoclinic, C-centered, with 102 atomic positions (possibly fractionally occupied) per cell. Our study of the Al-Co binary system includes for comparison purposes structures present in the Al-Fe and Al-Ni binaries (with Co substituting for Fe and Ni), and also the Al-Co-Ni ternary considered as a pseudobinary (substituting Co for Ni).

Spin polarization was considered but found to be present only at compositions  $x_{Co} > 0.5$ . The VWN spin-

interpolation [21] is used for the XC potential.

Given cohesive energies for all structures, we calculate enthalpies of formation by subtracting each cohesive energy from the tie-line joining each pure element in its lowest energy configuration. The structure (or coexistence of two structures) that minimizes the enthalpy is the thermodynamically stable structure for a given composition at low temperature. These form a “convex hull” of enthalpy versus composition, which we identify using the program qhull.

Our chief result is illustrated in Fig. 1. Evidently, we have nearly perfect agreement with the experimentally determined phase diagram. With the exception of the Al<sub>13</sub>Co<sub>4</sub> structures, all known low temperature phases lie on the convex hull. Likewise, the hypothetical structures drawn from chemically similar Al-Fe and Al-Ni systems lie above the convex hull. The faithfulness with which the experimental phase diagram is reproduced, and the ability to distinguish among chemically similar compounds is outstanding. All our data from this (and other) calculations is available on the WWW [22].

The sole area of discrepancy between our results and the experimentally reported phase diagram is in the range  $0.23 < x_{Co} < 0.26$ , precisely the area in which the experimental phase diagram is unsatisfactory in any case. Our calculated results can thus shed light on the experimentally unresolved questions. In particular, since we have no kinetic limitations on our ability to reach the energetically optimal structure, we may be able to distin-

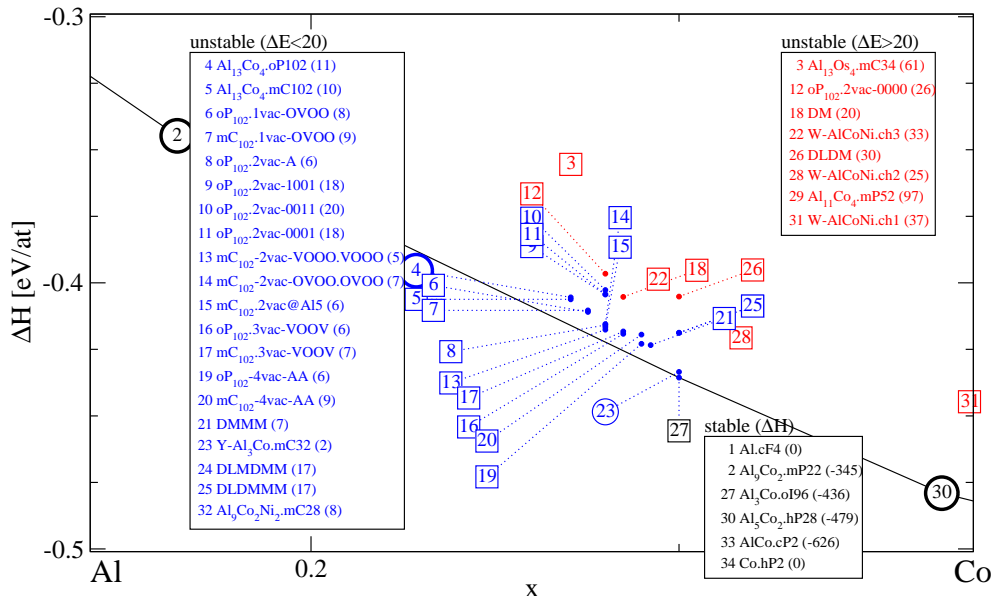


FIG. 2: Enthalpies of formation of  $\text{Al}_{1-x}\text{Co}_x$  over the range  $0.15 \leq x \leq 0.30$ . Notation as in Fig. 1

guish true low temperature phases from high temperature or metastable phases.

The main conclusion we draw is that the oP102/mC102 phases, believed stable at low temperatures, must be either metastable or high temperature phases, because they lie significantly above the convex hull. From our study of intrinsic configurational disorder in these structures we find a large configurational entropy sufficient to stabilize the oP102/mC102 above temperatures of about  $T = ?K$ . Thus we propose they are actually HT phases.

The Al<sub>3</sub>Co.oI96 structure, believed ???HT/MS???, lies essentially on the tie-line from Al<sub>9</sub>Co<sub>2</sub> to Al<sub>5</sub>Co<sub>2</sub>. It may be the true low temperature phase, or may be marginally unstable. Calculations employing the GGA [17] place it 2.6 meV/atom below the tie-line, implying stability, while calculations (not shown) employing the PBE place it 1.7 meV/atom above, indicating the range of uncertainty in calculated enthalpy differences. This discrepancy only affects oI96, the Al<sub>13</sub>Co<sub>4</sub> family remains unstable by about 5 meV/atom under all choices of XC potential.

### III. AL<sub>13</sub>CO<sub>4</sub> FAMILY

The two structures Al<sub>13</sub>Co<sub>4</sub>.oP102 and Al<sub>13</sub>Co<sub>4</sub>.mC102 share identical local building blocks and differ only in their global arrangement. To understand these structures it is helpful to use the elementary

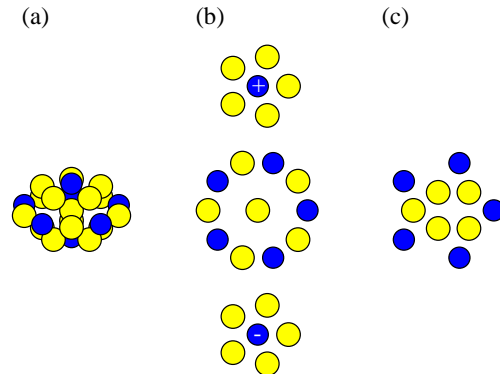


FIG. 3: PB cluster (a) 3D view of PB cluster. (b) exploded view showing Al-centered flat layer together with top and bottom caps marked, respectively, + and -. (c) PB junction layer.

cluster known as a pentagonal bipyramid [23, 24] (PB) illustrated in Fig. 3. The PB is a three-dimensional 23-atom cluster comprising a “flat” equatorial layer consisting of alternating Al and Co pentagonal rings centered by a single Al atom, and two “puckered” cap layers consisting of a small Al pentagon centered by a Co atom. The puckered layer Co atoms are displaced slightly away from their surrounding Al pentagons due to their repulsion from the PB center Al atom.

The stacking sequence of layers is thus the PB bottom tip (with a negative Co displacement marked “-”), next comes the PB center flat layer, then the PB top tip (with a positive Co displacement marked “+”) and finally a flat layer junction. The mean layer spacing is  $2 \text{ \AA}$ , and the 4 layers indicate an  $8 \text{ \AA}$  vertical periodicity. In the oP102/mC102 structures, layers are globally flat or puckered meaning that each flat layer consists entirely of PB centers and junctions, while each puckered layer consists entirely of PB +/- tips. Consider a “tube” of radius=PB radius centered on the PB central axis. Inside this tube the sequence of atoms is: PB tip (Co- at center), PB center (1 Al at center), PB tip (Co+ at center), PB junction.

All the Co atoms, and most of the Al atoms, are contained in PB clusters. This can be seen by examining Fig. 4. The remaining Al atoms are mainly located in flat “junction” layers, which join PB clusters stacked along the vertical direction. Each junction contains up to 5 Al atoms. In Fig. 4 some of these junction Al sites are labeled with numbers. Some flat layer Al atoms (e.g. numbers 5 and 14) are shared between neighboring clusters. Finally, there are 4 “glue” Al atoms in the puckered layers (labeled number 18) that do not belong to any clusters or junctions.

Viewing a single puckered layer, a tiling can be defined by joining Co atoms at PB tips. This particular structure contains only one type of tile, an elongated hexagon with edge length  $6.7 \text{ \AA}$ . At the same time, the flat layer exhibits a tiling by pentagons and rhombi, with edge length  $4.7 \text{ \AA}$ , formed by joining Co atoms.

It turns out that  $\text{Al}_{13}\text{Co}_4\text{.mC102}$  and  $\text{Al}_{13}\text{Co}_4\text{.oP102}$  define two different planar tilings of hexagon tiles (Fig. 5). Meanwhile, the pattern of Co displacements (equivalently the pattern of flat layers in which the PB is centered) assigns an “Ising” +/- spin to each vertex [24]. Finally, there can be vacancies which tend to concentrate among the Al atoms of PB junctions, as seen in Fig. 4. There are thus three important types of configurational freedom and associated disorder to consider: vacancies, layer puckering and tiling. We consider each of these in the following three subsections.

Also of interest is  $\text{Al}_{11}\text{Co}_4\text{.mP52}$ , a QC approximant with a  $4 \text{ \AA}$  periodicity [25]. This curious structure alternates motifs similar to the flat and puckered layers of mC102 and oP102, but with only a  $4 \text{ \AA}$  periodicity so that the “flat” layers cannot be perfect mirrors, and hence are not perfectly flat. We find it is quite high in energy, and also that both layer types relax to a perfectly flat structure.

### A. Vacancy disorder

The structure determinations [12, 13] of  $\text{Al}_{13}\text{Co}_4\text{.mC102}$  reported partially occupied Al sites, especially among PB junction sites in the flat layers. The partially occupied sites are shaded and labeled in

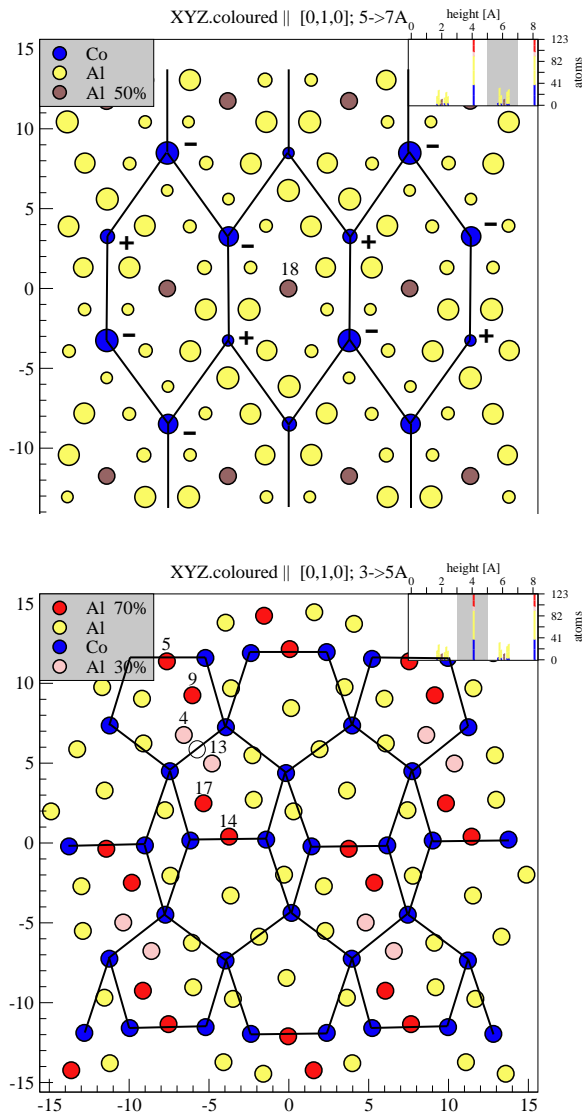


FIG. 4: Puckered (top) and flat (bottom) layer structures of  $\text{Al}_{13}\text{Co}_4\text{.mC102}$ . Blue atoms are Co, yellow are Al, while red, brown and pink indicate fractional occupancy of 0.7, 0.5 and 0.3, respectively according to the structure determination of Hudd. Numbers are orbit labels. Large/small atoms indicate displacement down/up.

Fig. 4. Vacancies are not reported in recent evaluation oP102 [11], but abnormally large thermal factors in those structures may indicate partial occupancy. Vacancies are plausible because these sites are overcrowded, with Al-Al spacing as low as  $2.3 \text{ \AA}$ , where  $2.9$  would be more favorable. In this section we explore the role of vacancies from both an electronic structure and statistical mechanical point of view. We show that a small number of vacancies lowers the enthalpy, but not sufficiently to yield low temperature stability. However, when vacancy entropy is included the structure could achieve high temperature stability.

First we examine the vacancy energetics. Inspecting

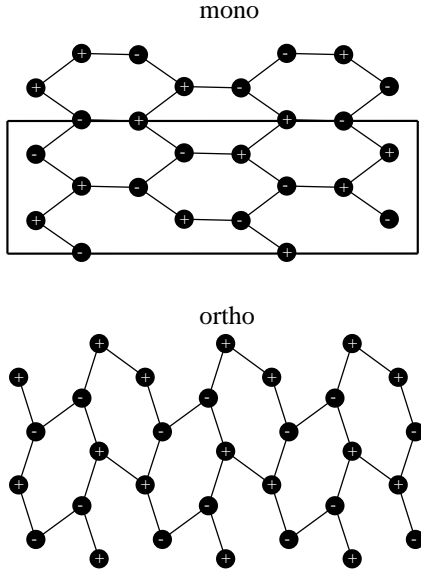


FIG. 5: tilings and puckering patterns of mC102 and oP102. Labels in oP102 indicate the set of independent vertices for studies of puckering.

Fig. 2 reveals that a few vacancies can lower the enthalpy, with  $\Delta E$  dropping from +12 meV/atom to +6 meV/atom. Limited vacancy formation can be understood from the perspective of electronic structure by inspecting the electronic density of states illustrated in Fig. 6. Notice that the density of states contains a strong pseudogap near the Fermi energy. For fully occupied  $\text{Al}_{13}\text{Co}_4$ .mC102 the Fermi energy lies just to the right hand side of the gap. Introducing Al vacancies moves  $E_F$  towards the bottom of the pseudogap, which can lower the band structure energy.

The pseudogap has a steep left side and a relatively shallow right side. This can explain the trend in stability of mC102 For Al-TM alloys with TM a first-row transition metal. Recall that the sequence of chemical valence runs .... Mn, Fe, Co, Ni .... The Fermi energies in Fig. 6 were calculated within the rigid band model. In a 102 atom unit cell of  $\text{Al}_{13}\text{Co}_4$ , with stoichiometry  $\text{Al}_{78}\text{Co}_{24}$ , replacing Co with Mn, Fe or Ni changes by total number of electrons by -48, -24 or +24, respectively. We calculated the DOS for fully occupied  $\text{Al}_{13}\text{Co}_4$ .mC102, then integrated the DOS from  $E_F(\text{Co})$  up or down to the energy that would match the change in electron count.

When TM=Mn, the structure is electron-poor and  $E_F$  lies well below the gap. mC102 is energetically unfavorable. When TM=Fe,  $E_F$  lies at a nearly optimal point just at the left hand edge of the gap. Indeed, our calculations [22] reveal that mC102 is stable at low temperature in  $\text{Al}_{13}\text{Fe}_4$ , and vacancies are unfavorable. When TM=Co, the structure becomes slightly electron-rich.

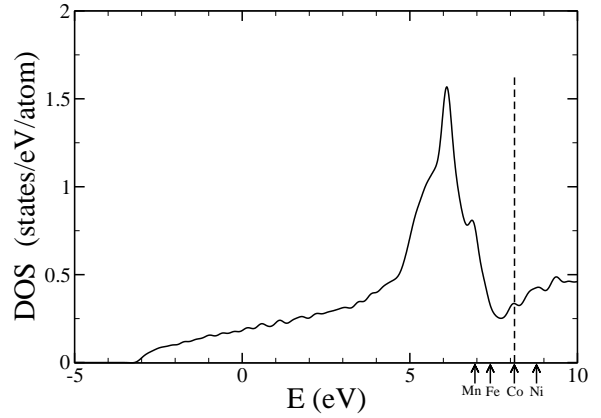


FIG. 6: DOS of fully occupied  $\text{Al}_{13}\text{Co}_4$ .mC102. Arrows indicate  $E_f$  for  $\text{Al}_{13}\text{TM}_4$  with (lowest to highest) TM=Mn, Fe, Co, and Ni calculated within the rigid band model.

Low temperature stability is lost and vacancies are favored. Finally, when TM=Ni  $E_F$  moves above the pseudogap and mC102 is energetically unfavorable.

The distribution of vacancies among Aluminum atoms in mC102 (see shading in Fig. 4) and oP102 provides a source of configurational entropy. We analyze this in detail for mC102, but similar results are found for oP102. The string of six shaded Al atoms that lie in the flat layer, where two PB junctions occur side-by-side, is overly dense in Al. The entire string of six is reported to be partially occupied according to Hudd, but only the inner four atoms are partially occupied according to Freiburg. In this string we find Al spacings as low as 2.31 Å. For comparison the peak of the AlAl pair correlation function in mC102 occurs at 2.83 Å. All six of these sites are found partially occupied in the structure solution of Hudd [12]. Only the inner four possess vacancies according to the structure solution of Freiburg [13].

We investigated the stability and energetics of structures with Al vacancies inserted at these sites (see Fig. 2) and found that removal of one or two Al out of the string of six is favorable. It turns out that introduction of vacancies at the endpoints of the string of 6, at sites of type [13] Al3, leads to large displacements of the neighboring Al6 atoms to fill the vacancy. The Al3 vacancies are thus unstable, consistent with Freiburg's observation of full occupancy. A puckered layer site, Al15 is partially occupied according to Hudd but not Freiburg. We found the vacancy at this site to be mechanically stable, but energetically costly (1.5eV per vacancy).

The other vacancies, at sites Al6 and Al7 are energetically favorable, reducing  $\Delta E$  from +10.1 meV/atom to, respectively, +5.9 and +6.7 meV/atom. Vacancies at Al6 sites are mechanically stable, with only small relaxations of adjacent atoms. In contrast, when an Al7 site is vacant the adjoining Al7 atom displaces towards the midpoint of the bond that joins them. The resulting positions lie slightly off the midpoint at the locations indicated with open circles in Fig. 4.

To gauge the thermodynamic impact of Al vacancies, we evaluate the partition function

$$Z = \sum_{config} \exp -(\Delta E)/k_B T. \quad (1)$$

We restrict our sum to the set of configurations containing just one vacancy per 51-site primitive cell and include only the vacancies at Al6 and Al7 sites. From the partition function we obtain the free energy, enthalpy, entropy and heat capacity by the usual methods of statistical mechanics.  $G = -k_B T \log Z$ ,  $S = -\partial G/\partial T$ ,  $H = G + TS$ ,  $C_p = T\partial S/\partial T$ .

If the reduction in free energy due to vacancy entropy at high temperature exceeds the unfavorable enthalpy of mC102 compared with Al9Co2.mP22 and Al5Co2.hP28, then vacancy disorder can lead to high temperature thermodynamic stability of mC102. Implicitly we assume vacancy entropy can be neglected in mP22 and hP28 (our calculations find the vacancy formation energy is ?). We also assume the vacancy entropy of mC102 is large compared to any differences in vibrational entropy among these structures. Because the terms in eq. 1 are weighted according to  $\Delta E$ , the enthalpy difference between our vacancy structures and the tie-line connecting mP22 to hP28, thermodynamic stability occurs if  $G < 0$ .

As temperature rise up to the peritectic melting temperature  $T_m=1366K$ , we see that TS approaches E but does not reach it. To stabilize Al<sub>13</sub>Co<sub>4</sub>, an additional effect is needed, which turns out to be the vibrational entropy of low frequency phonons (see Sect. IV).

Regardless of the high temperature stabilization mechanism, our study of vacancy energetics shows that neither Al<sub>13</sub>Co<sub>4</sub>.mC102 nor Al<sub>13</sub>Co<sub>4</sub>.oP102 is stable at low temperature at any composition. Our results also indicate that 2-4 Al vacancies per 102 atom cell are favorable in both Al<sub>13</sub>Co<sub>4</sub>.mC102 and Al<sub>13</sub>Co<sub>4</sub>.oP102, placing their phase fields slightly to the right of  $x=0.2353$ . Vacancies are favored owing to the crowding of Al atoms in flat layers and to the location of the Fermi energy slightly above a pseudogap.

## B. Puckering disorder

We can define Ising model couplings between neighboring tiling vertices by exhaustively forming all spin patterns on the vertices of a single unit cell and comparing their energies. To eliminate coupling between the puckering pattern and the distribution of vacancies among junction layer Al atoms, we adopt a simple rule that places a single Al atom midway between sites of types 4 and 13 (see Fig. 4). In this way, a single Al atom lies in each flat layer along each hexagon tile edge. This rule can be applied to either mC102 or oP102, but we choose to focus on oP102. The unit cell contains 100 atoms and 2 vacancies.

Our results, which are visible in Fig 2 and summarized in Table I, can be fit using only two coupling con-

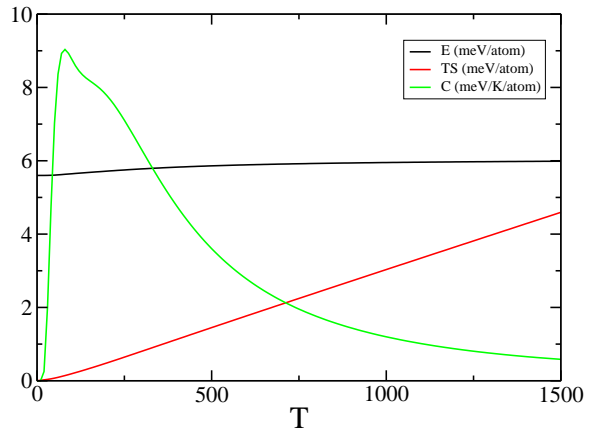


FIG. 7: Vacancy heat capacity, internal energy and entropy.

TABLE I: Puckering pattern energies.

Pattern	+J1	-J1	+J2	-J2	$\Delta E$	fit
0000	6	0	4	0	20.3	22.1
0001	3	3	2	2	12.1	11.6
0011	4	2	0	4	13.7	8.9
0101	2	4	0	4	0	5.0
1001	0	6	4	0	12.0	10.5

stants  $J_1$  and  $J_2$ , both antiferromagnetic, and an overall constant  $J_0$ . We set  $\Delta E = J_0 + J_1 N_1 + J_2 N_2$  with  $J_0 = 11.6$ ,  $J_1 = 1.0$ ,  $J_2 = 1.2$ . Since both  $J_1$  and  $J_2$  are antiferromagnetic, the ordering is partially frustrated. Still, a unique ground state pattern exists and matches the experimentally observed pattern, for both oP102 and mC102.

To investigate the possibility of puckering disorder contributing to the entropy, we need to generalize our Ising model to three dimensions. This is because the entropy of in-plane disorder grows like the  $2/3$  power of volume and hence is subextensive. Thus we consider stacking disorder in the puckering sequence along a column of PB's.

Reversal of the puckering sequence is created by placing 2 Al atoms inside two consecutive flat layers, averaging the structure of a 1 Al PB center and a 3 Al junction layer. The energy cost for this reversal is ? eV which we take as the strength of vertical coupling  $Jz$  in our Ising model.

Given our couplings we can evaluate the statistical mechanics of the Ising model representing our structures. The tiling pattern of mC102 is topologically equivalent to a honeycomb lattice (what about OP102?) (near-neighbor coupling J1) with added horizontal J2 couplings. This lattice is then stacked along the  $c$  axis at 4 Å intervals and coupled with the vertical coupling  $Jz$ . It turns out that the phase transition in this model occurs around  $T=?K$ , far above the actual melting point of  $T=1366K$ . We conclude that disorder in the puckering pattern is of no thermodynamic significance for mC102, and presumably for oP102 as well.

### C. Tiling disorder

Note in Fig. 2 how close mC102 and oP102 are in energy. This near degeneracy persists across a broad range of composition, and suggests that perhaps any tiling of the plane by hexagons would be nearly as good.

## IV. VIBRATIONAL PROPERTIES

We calculated the vibrational density of states and vibrational free energy of the main Al-Co compounds. Including the vibrational free energy allow us to extend our knowledge of stability from the limit of vanishing temperature, where only the enthalpy is relevant, to finite temperature. It turns out that  $\text{Al}_{13}\text{Co}_4$  exhibits a small excess of low frequency modes associated with the disordered flat layer Aluminum atoms. These contribute sufficient vibrational entropy that, combined with the previously identified configurational entropy of vacancies, is sufficient to stabilize the quasicrystal approximant structure at elevated temperature.

To calculate the vibrational density of states, a complete set of independent atomic displacements was performed within single primitive cells of each structure. For  $\text{Al}_{13}\text{Co}_4$  we chose a 51-site primitive cell of mC102, with a single Al vacancy at position #13. The forces were fit to a mass and spring model, including bond stretching and bending in the harmonic approximation, using the “fitfc” method of the ATAT toolkit [26]. The vibrational DOS was then calculated using a full Brillouin Zone integration, so that the structural details in the resulting DOS are true intrinsic properties of the model.

Fig. 8 illustrates the results. Of particular interest is the comparison between  $\text{Al}_{13}\text{Co}_4$  and the competing crystal structures  $\text{Al}_9\text{Co}_2$  and  $\text{Al}_5\text{Co}_2$ . Note the slight excess density of states at low frequency in  $\text{Al}_{13}\text{Co}_4$ . Such an excess is observed experimentally MAREK: CITE WHO?. We attribute these modes to flat-layer Al atoms because they disappear when the flat layer sites are fully occupied.

Vibrational free energies are calculated as

$$f_{\text{vib}}(T) = k_B T \int \text{DOS}(\omega) \log 2 \sinh \hbar\omega/2k_B T d\omega \quad (2)$$

Low frequency modes that can be excited at low temperatures contribute strongly to the vibrational entropy, reducing the free energy. The difference between the vibrational free energy of  $\text{Al}_{13}\text{Co}_4$  and a composition-weighted average of the free energies of  $\text{Al}_9\text{Co}_2$  and  $\text{Al}_5\text{Co}_2$  is plotted in Fig. 9. Evidently, the low frequency modes of  $\text{Al}_{13}\text{Co}_4$  lend it thermodynamic stability as temperature rises. The free energy reduction reaches 7 meV/atom at the melting temperature  $T_m=1366\text{K}$ .

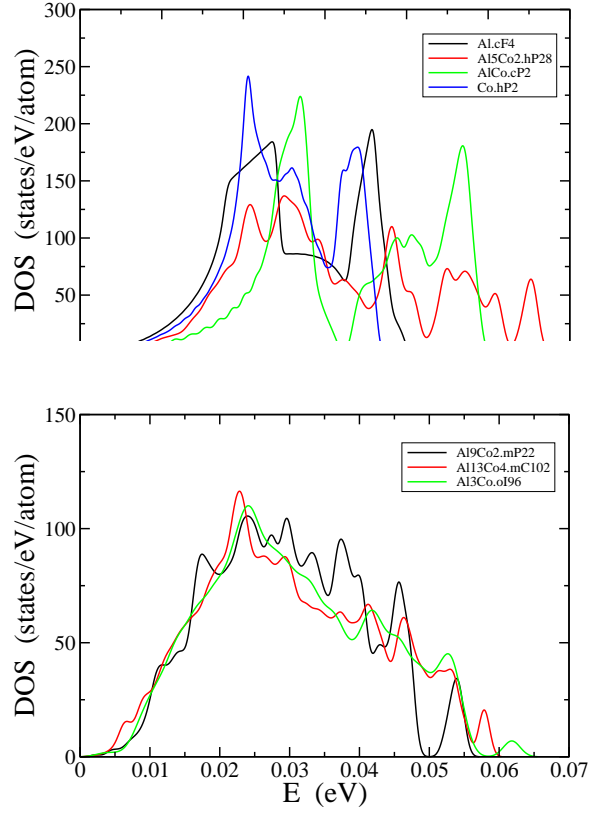


FIG. 8: Vibrational densities of states for Al-Co compounds. We separate those of composition  $0.1818; x_{\text{Co}}; 0.25$  from the rest

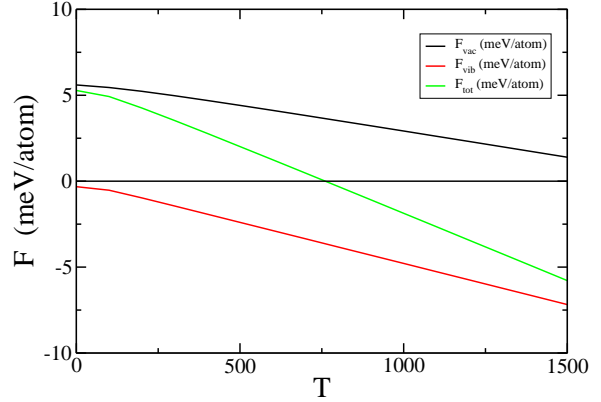


FIG. 9: Vacancy, vibrational and total free energy

## V. MOLECULAR DYNAMICS

Given the presence of vacancies and associated low frequency phonons, we performed a molecular dynamics simulation for a single 102-site unit cell of  $\text{Al}_{13}\text{Co}_4$ .mC102. We introduced vacancies at the initial positions of site class #13, and evolved the system at  $T=1350\text{K}$  for 8.5 picoseconds. Forces were calculated from first-principles using VASP. Fig. 10 illustrates the result by projecting the trajectories of all atoms in the

two layers illustrated in Fig. 4 into a plane. MAREK: NEED TO SHIFT/CROP THIS FIGURE FOR CONSISTENCY WITH FIG 4. Clearly Al atoms diffuse easily along the channels defined by the strings of four Al atoms where the vacancies occur.

Rather than decompose the entropy into separate vacancy and vibrational contributions (a decomposition the is clearly defined only in the limit of low temperature), we could estimate the combined entropy directly by treating the string of Al atoms as a liquid. Treat Al atoms as hard spheres of diameter  $a = 3 \text{ \AA}$ . A string of four Al atoms defines a channel of length  $12 \text{ \AA}$ , which will be occupied by three spheres. The translational partition function may be evaluated as

$$Z_{liquid} = \frac{1}{\Lambda^3} \int_0^a dx_1 \int_{x_1+a}^{2a} dx_2 \int_{x_2+a}^{3a} dx_3 = \frac{9}{2} \left(\frac{a}{\Lambda}\right)^3 \quad (3)$$

The thermal de Broglie wavelength

$$\Lambda = \sqrt{\frac{2\pi mk_B T}{h^2}} = .09 \text{ \AA} \quad (4)$$

at  $T=1350\text{K}$ . In contrast, if the atoms remained bound within a distance  $b$  of their nominal lattice positions, we can estimate the partition function of each Al atom as

$$Z_{solid} = \frac{1}{\Lambda^3} \left(\int_{-b}^b dx\right)^3 = (b/\Lambda)^3 \quad (5)$$

From Fig. 10 it appears that  $b \approx 0.5 \text{ \AA}$ . From the partition functions we calculate the free energy as  $F = -k_B T \log Z$ . Putting in numbers for  $T=1350\text{K}$ , and dividing by 50 (the number of atoms in the primitive cell containing a single Al string) we find  $F_{liquid} = .024 \text{ eV/atom}$ , and  $F_{solid} = .010 \text{ eV/atom}$ . So the liquid entropy lowers the free energy below the solid by about  $10 \text{ meV/atom}$ , consistent with our prior estimates.

## VI. $\text{Al}_3\text{Co}$ VARIANTS

Several structures,  $\text{Al}_{13}\text{Co}_4.\text{mC32}$ ,  $\text{Al}_{13}\text{Os}_4.\text{mC34}$  and  $\text{Al}_3\text{Co.oI96}$  are closely related and seem plausible for compositions around  $\text{Al}_3\text{Co}$ . They all may be viewed as different stackings of the same average layer with slight modifications. The layer modifications are denoted D for dense, M for medium and L for loose. D has 13 Al, M has 12 Al and L has 10 Al. The mC34 structure is DD, mC32 is MM and oI96 is DLDDLD. Relative horizontal translations of the layers lead to either monoclinic or orthorhombic structures. Inspecting the patterns of large Co (outlined) reveals partial PB's. Roughly speaking the PB equators correspond to L layers, fully occupied PB junctions correspond to D layers. The M layer corresponds to a PB junction with the sites labeled 4 and 13 replaced by their average position as illustrated in Fig. 4.

The structure we label as  $\text{Al}_{13}\text{Co}_4.\text{mC32}$  has not actually been reported in the literature in the Al-Co binary system. Rather, it appears in the Al-Co-Ni ternary

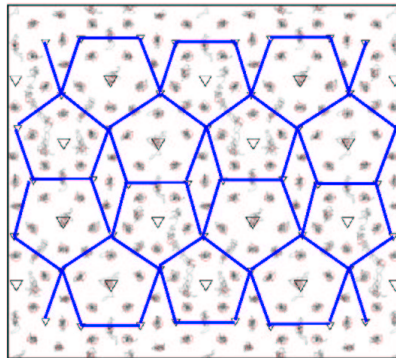


FIG. 10: Projected molecular dynamics trajectories. Flat layer tiling indicated in blue, Al and TM atom positions indicated via red circles and black triangles, respectively.

as the “X” phase (Steurer and Zhang) and is given structure  $\text{Al}_{13}(\text{Co},\text{Ni})_4.\text{mC34-1.8}$ . The notation mC34-1.8 indicates the introduction of 1.8 vacancies into the  $\text{Al}_{13}\text{Os}_4.\text{mC34}$  structure. The X phase extends almost to the Al-Co binary, with Ni content as low as 3% Ni. The structure we label  $\text{Al}_3\text{Co.oI96}$  also comes from the ternary, reported [27] as the “ $Y_2$ ” phase of  $\text{Al}_9\text{Co}_2\text{Ni.oI96}$ .

Our results as displayed in Fig. 2 show that the fully occupied  $\text{Al}_{13}\text{Os}_4.\text{mC34}$  structure is highly unfavorable, suggesting that atoms are too crowded in the dense D layers. Relieving the overcrowding by replacing D with M leads to the far more stable structure we refer to as  $\text{Al}_{13}\text{Co}_4.\text{mC32}$ . Because each of these structures has a  $4 \text{ \AA}$  repeat, each atomic layer is forced to be a mirror plane, and hence flat.

The most favorable of all,  $\text{Al}_3\text{Co.oI96}$ , mixes D and L layers, with a stacking sequence of  $12 \text{ \AA}$  periodicity. In this sequence, the D layers are puckered and the L layers flat. Apparently puckering of the D layer reduces overcrowding resulting in a favorable energy.

According to the data presented in Fig. 2, the enthalpy of oI96 is so low that it reaches the convex hull indicating low temperature thermodynamic stability. However, it just barely touches the hull, lying  $1.8 \text{ meV/atom}$  below the tie-line joining mP22 to hP28. Hence its sta-

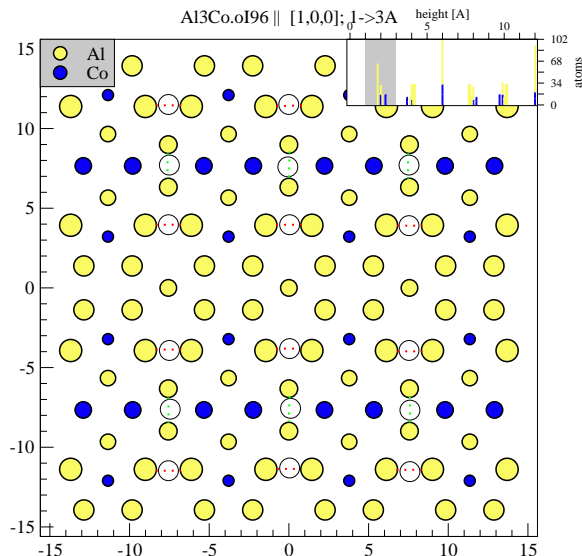


FIG. 11: Dense “D” layer of  $\text{Al}_3\text{Co.oI96}$ . Convert to medium “M” by replacing Al pairs on vertical (green) bonds with single Al at center. Convert to loose “L” layer by replacing in addition horizontal (red) bonds. Fragments of an imperfect pentagon-rhombus tiling are outlined.

bility is barely resolved within the expected accuracy of our methods. Indeed, using a different exchange correlation function, the PBE [28] instead of the PW91 [17], results in an energy 2.0 meV/atom *above* this tie-line. We therefore refrain from predicting that oI96 is actually a low temperature phase. Rather we suggest that further experiments are needed to determine if either mC32 or

oI96 is stable, and over what temperature range.

Also in the ternary, but close to the binary Al-Co axis, there is a quasicrystal approximant  $\text{W-AlCoNi.mC578}$ , with lattice parameters  $39.67 \times 8.15 \times 23.39$  Å at composition  $\text{Al}_{72}(\text{Co,Ni})_{28}$ . The pseudo 10-fold axis is parallel to  $b$  (lattice parameter 8.15 Å). This occurs close to the composition of the “basic Co-rich” decagonal phase, which also features an 8 Å stacking periodicity, and is presumably close in structure. The W phase structure contains mixed Al/TM occupancy sites. We assigned all  $\text{TM}=\text{Co}$ , and resolved the mixed occupancy in various ways, the most Al-rich of which we include in Fig. 2. Evidently this structure is rather far from low temperature stability as a binary. Indeed, even in the ternary we find it is not LT stable.

## VII. DISCUSSION

We calculated cohesive energies for many structures in the binary Al-Co alloy system. Our results generally support the main features of the experimentally assessed phase diagrams at low temperatures, but disagree in some details. The disagreements come entirely in a small composition range where recent experimental investigations have revealed new and conflicting results.

### Acknowledgments

This work was supported in part by NSF grant DMR-0111198.

- 
- [1] (????), alCo binary metastable DQC.  
 [2] (????), alCoNi stable DQC.  
 [3] T. B. Massalski et al., eds., *Binary alloy phase diagrams* (ASM International, Ohio, 1990).  
 [4] T. Goedecke, *Z. Metallkd.* **62**, 842 (1971).  
 [5] T. Goedecke and M. Ellner, *Z. Metallkd.* **87**, 854 (1996).  
 [6] T. Goedecke, *Z. Metallkd.* **88**, 904 (1997).  
 [7] B. Grushko, R. Wittenberg, K. Bickmann, and C. Freiburg, in *Proc. of the 5th Int. Conf. on Quasicrystals*, edited by C. Janot and R. Mosseri (World Scientific, Singapore, 1995), pp. 684–7.  
 [8] B. Grushko, C. Freiburg, K. Bickmann, and R. Wittenberg, *Z. Metallkd.* **88**, 379 (1997).  
 [9] B. Grushko, R. Wittenberg, K. Bickman, and C. Freiburg, *J. Alloys Comp.* **233**, 279 (1996).  
 [10] H. Okamoto and T. B. Massalski, *Desk Handbook: Phase Diagrams for Binary Alloys* (ASM International, Ohio, 2000), chap. Impossible and improbable alloy phase diagrams.  
 [11] J. Grin, U. Burkhardt, M. Ellner, and K. Peters, *J. Alloys Comp.* **206**, 243 (1994).  
 [12] R. C. Hudd and W. H. Taylor, *Acta Cryst. A* **15**, 441 (1962).  
 [13] C. Freiburg, B. Grushko, R. Wittenberg, and W. Reichert, *Mat. Sci. Forum* **228-231**, 583 (1996).  
 [14] G. Kresse and J. Hafner, *Phys. Rev. B* **47**, RC558 (1993).  
 [15] G. Kresse and J. Furthmüller, *Phys. Rev. B* **54**, 11169 (1996).  
 [16] G. Kresse and D. Joubert, *Phys. Rev. B* **59**, 1758 (1999).  
 [17] J. Perdew and Y. Wang, *Phys. Rev. B* **45**, 13244 (1992).  
 [18] M. Mihalkovič and M. Widom, sub. to *Phys. Rev. B* (2004), cond-mat/0405298.  
 [19] P. Villars, *Pearson’s Handbook, Desk Edition* (ASM International, Materials Park, Ohio, 1997).  
 [20] Recent AlCo structure determinations (????).  
 [21] L. W. S.H. Vosko and M. Nussair, *Can. J. Phys.* **58**, 1200 (1980).  
 [22] M. Mihalkovič and M. Widom, web site (2004), <http://alloy.phys.cmu.edu>.  
 [23] C. L. Henley, *J. Non-Cryst. Solids* **153-154**, 172 (1993).  
 [24] E. Cockayne and M. Widom, *Phil. Mag. A* **77**, 593 (1998).  
 [25] X. Z. Li, N. C. Shi, Z. S. Ma, X. L. Ma, and K. H. Kuo, *Phil. Mag. Lett.* **72**, 79 (1995).  
 [26]  
 [27] Y. Grin, K. Peters, U. Burkhardt, K. Gotzmann, and M. Ellner, *Z. Krist.* **213**, 364 (1998).  
 [28] J. P. Perdew, K. Burke, and M. Ernzerhof, *Phys. Rev.*

Lett. **77**, 3865 (1996).